Aerodynamic Analysis and Design of a Mars Rotor with Tandem Airfoil Configurations

Ricson Thanolil Rejimon*, Thomas Homer*, Cheng Chi
University of the West of England, Bristol, United Kingdom
Lex.Chi@uwe.ac.uk

1 INTRODUCTION

This study explores the potential aerodynamic benefits of tandem airfoil configuration in rotors operating in the Martian atmosphere. Ever since the inspiring successful flight of the JPL/NASA/AeroVironment Mars Helicopter (MH) Ingenuity on Mars in 2021, the new way of Mars exploration has been proven feasible and opportunities have opened up for science missions. To carry out actual science missions with planetary aerial vehicles, the next generation of Mars Science Helicopter (MSH) with large range and payload is under development via the Rotor Optimization for the Advancement of Mars eXploration (ROAMX) project [1] based on the conceptual design (Figure 1) proposed by NASA Ames and JPL [2].

In the past decade, there has been significant progress in the technologies at multiple levels that are necessary for the development of the next-generation Mars helicopter. At the airfoil level, Winslow et al. [3] systematically investigated the performance of airfoils at these low Reynolds numbers, and Koning et al. [4, 5] evaluated the performance improvement of cambered flat plate airfoil on the MH rotor as well as performed airfoil optimization in low-Re regime which leveraging the large-scale vortex shedding phenomenon. Experimental investigations of unconventional airfoils were done by Munday et al. [6] (triangular airfoil) and Koning et al. [7] (clf5605 airfoil used on MH and roamx-0201 type airfoil designed by the ELISA optimization framework [8]) in the Tohoku University Mars Wind Tunnel. At the blade and rotor level, Chi and Lumba [9, 10] designed the internal structure of MSH blades and analyzed the structural dynamic characteristic and aero-structure interaction during hover and forward flight. The blades were then built for further testing within the ROAMX project [1]. As for the studies at the full aircraft level, Grip et al. [11] developed the flight dynamic model of MH and analyzed the stability and controllability.

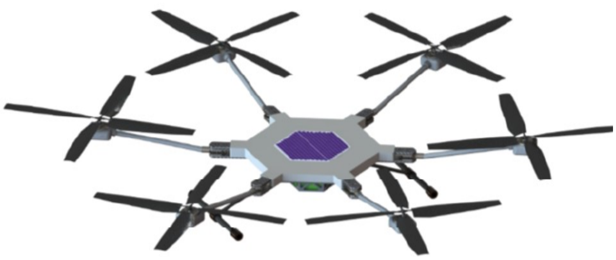

Figure 1: Mars Science Helicopter hexacopter configuration by NASA.

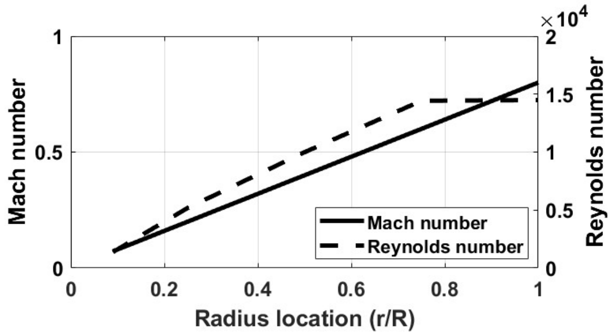

Figure 2: Re and Ma of the hexcopter rotor in hover.

Though there is progress, challenges remain in aspects such as relatively low rotor performance (Figure of Merit about 0.65 [4]) compared to Earth's counterpart (Figure of Merit about 0.8); the low atmosphere density results in low damping flap motions which leads to difficulties in stable flight control [11]; Weight increased due to: the need of increasing flap frequency for a more controlable rotor system, the additional weight needed to counter the blade propeller pitch moment due to the thin airfoil which limiting the space for leading edge weight, and the structure to withstand the high tensile loading due to the high rotational speed [9].

The need to overcome the challenges mentioned above combined with the development of tandem airfoil configuration research in low Re leads to the focus of this study. In the harsh Martian atmosphere, the MSH rotor operating flow conditions are characterized by low chord-based Reynolds number ($Re = 10^3 - 10^4$) driven by low density, and high subsonic Mach number ($Ma = 0.8$) near the tip due to the lower speed of sound and high rotational speeds, as shown in Figure 2. This is a rare flow condition for aircraft operating in Earth's atmosphere, therefore there is limited precedent research. However, research shows the advantages of tandem airfoil configurations in low Reynolds number flow. Scharpf and Mueller [12]

*The authors contribute equally to this paper.

studied the low Re (8.5×10^4) airflow over a wing with tandem airfoil configuration at various angles of attack. Their findings revealed that the upstream airfoil facilitated attached flow on the downstream airfoil at high angles of attack leading to an enhancement of the lift-to-drag ratio (L/D). Broering and Lian [13] studied the aerodynamics of flapping wings in tandem configuration to search for the optimal wing spacing for max lift and thrust. Jones et al. [14] investigated various tandem arrangements of two flat plates in low Re (10^5). The influence of varying the vertical and horizontal spacing between the wings and the airfoils' angles of attack were investigated showing lift increase and stall delay. Faure et al. [15, 16] examined the flow of tandem airfoil configurations experimentally (wind tunnel and Particle Image Velocimetry) and analytically to identify the configuration that generates maximum lift.

Most of the studies carried out on tandem configuration focused on 2D airfoils or fixed wings. There is a gap in the understanding of the impact of tandem airfoil configurations on rotors. Hence, a systematical study was performed to understand the influence of tandem airfoil configuration on Mars rotors and identify the configuration that can improve hover or forward flight performance. The parameters of the tandem airfoil configuration, shown in Figure 3, are gap (G = normal distance between the $1/4c$), stagger (S = chordwise distance between the $1/4c$), and decalage (α_D = angle between the chord lines). A conceptual rotor blade with tandem airfoil configuration (simplified by using a uniform airfoil) is shown in Figure 4. Within a blade, the upstream and downstream blades are connected at the tip and the root. The tandem airfoil configuration also has potential impacts on the rotor structural dynamic and controllability. Though they are beyond the scope of the current study, this study lays a good foundation for the investigation of other aspects of Mars rotors.

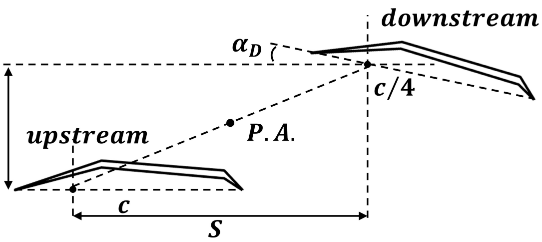

Figure 3: Tandem airfoil configuration parameters.

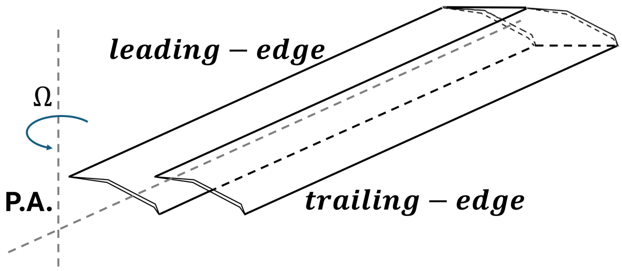

Figure 4: Rotor blade with tandem airfoil.

2 METHODS

2.1 Airfoil analysis (Ricson,Thomas)

The airfoil Computational Fluid Dynamics (CFD) analysis is carried out by ANSYS FLUENT. The grid of a tandem airfoil is shown in Fig. 5. Since the MSH rotor airfoil studied has sharp leading and trailing edges, particular care was taken to resolve the edges properly, and an unstructured mesh was used. The airfoil mesh and simulation parameters are presented in Table. 1. The number of nodes in the wrap-around direction for a single airfoil is 966. The initial layer thickness and the growth rate are set to ensure the mesh within the boundary layer is fine enough. The outer boundary was placed 20 chord lengths away from the airfoil. A shear stress transport (SST) $k-\omega$ turbulence model is used to perform the transient analysis. The flow condition used in each airfoil analysis corresponds to the MSH blade section Re, Ma calculated base on the Mars atmosphere property (density 0.015 kg/m^3, speed of sound 233.1 m/s, dynamic viscosity $1.12 \times 10^{-5} Ns/m^2$). The upstream and downstream airfoil's lift, drag, and pitch moment (C_l, C_d, C_m) are combined and non-dimensionalized into coefficients following the Equations (1)- (4) for comparison and rotor analysis. The pitch moment coefficient of the tandem airfoil is separated into two parts: C_{m_0} the combined pitch moment and C_{m_F} the force-related moment.

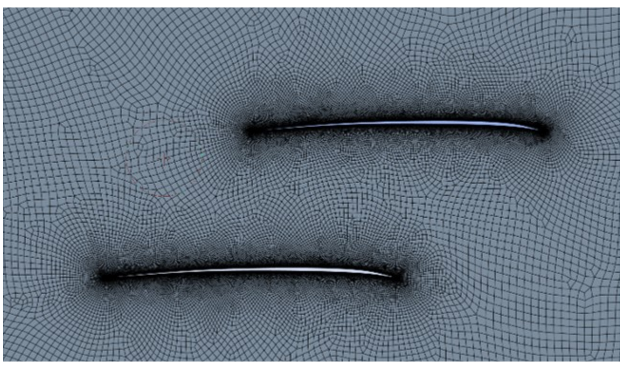

Figure 5: Mesh for a tandem airfoil ($G = 0.5c$ $S = 0.5c$).

Table 1: Airfoil simulation parameters.

	Parameters
Meshing	ANSYS Meshing
Mesh type	C-H unstructured
Surface nodes	966
1^{st} layer thickness	0.0000785 m
Growth rate	1.08
Boundary layer thickness	0.0162 m
Solver	ANSYS FLUENT 24
Turbulence model	SST $k-\omega$
Solution type	2D
Settings	double precision transient pressure-based

update to CH hybrid mesh

$$C_l = \frac{S_u C_l^u + S_d C_l^d}{S_u + S_d} \quad (1) \qquad C_d = \frac{S_u C_d^u + S_d C_d^d}{S_u + S_d} \quad (2)$$

$$C_{m_0} = \frac{S_u c_u C_m^u + S_d c_d C_m^d}{S_u c_u + S_d c_d} \quad (3) \qquad C_{m_F} = \frac{2(S_u C_F^u f - S_d C_F^d (1-f))}{S_u + S_d} \quad (4)$$

where c_u and c_d are the chords, and S_u and S_d are the areas of the upstream and downstream sections, respectively; f the faction of the distance from the upstream quarter-chord point to the pitch axis over the distance between two quarter-chord points; C_F^u and C_F^d the force coefficient of upstream and downstream airfoils normal to the line connecting the quarter-chord points.

To systematically understand the influence of tandem airfoil configuration on aerodynamic performance under Martian conditions, a comprehensive parametric study was conducted. This involved varying three primary parameters: *gap (G)*, *stagger (S)*, and *decalage angle* (α_D) — as defined in Figure **??**. The simulations aimed to capture the effects of these parameters on lift (C_l), drag (C_d), and pitching moment (C_m), ultimately informing the rotor performance models used later in this study.

The CFD simulations were organized into three sweep categories:

- **Gap Variation:** Keeping stagger and decalage fixed, the vertical separation (G) between the quarter-chord points of the upstream and downstream airfoils was varied from negative to positive values. This assessed the aerodynamic impact of placing the upstream airfoil either above or below the downstream airfoil.
- **Stagger Variation:** With gap and decalage held constant, the chordwise offset (S) was varied from 0 to 1.5 chord lengths. This helped evaluate how streamwise spacing affects wake interaction and load distribution between the airfoils.
- **Decalage Angle Study (α_D):** After identifying promising configurations from the gap-stagger sweep, we introduced variation in the relative angle between the airfoils. This was used to assess its role in lift enhancement, flow attachment, and potential moment balancing strategies.

Each case was simulated in ANSYS FLUENT using the same mesh resolution and solver settings described previously. To ensure consistency across simulations:

Ricson, Please include the arifoil Cl Cd figures that compared with my previous CFD data. Point out that this is a sanity check, not a validation.

- airfoil shape (double-sharp-edge profile at 75%R) and conditions (Mars atmospheric properties) were fixed.
- simulations were **transient and 2D**, using the **SST** k–ω turbulence model.
- ases assumed zero inflow angle, isolating the effect of configuration geometry on aerodynamic coefficients.

What does zero inflow angle mean? Angle of attach sweep are done.

tcomes of this study provided trends that directly influenced the rotor modeling strategy. For instance, it was placing the upstream airfoil *above* the downstream airfoil (negative gap) and using a stagger around one chord length led to improved maximum lift coefficient, while the opposite configuration generally degraded performance. These findings were incorporated into the rotor-level BEMT analysis by using combined airfoil polars as discussed in Section 2.2.

No discussion in this section. Please move it to section 3 or 4.

2.2 Rotor modeling (Thomas, Lex)

The baseline rotor used in this study is the MSH hexacopter four-bladed rotor with a radius of R = 0.64 m, a solidity of σ = 0.142. The blade airfoils are shown in Figure 6. Two 8% thickness-to-chord diamond airfoils are used at 9%R and 25%R. Two 1% thickness-to-chord double sharp edge airfoils are used at 50%R and 75-100%R. The chord and the built-in twist distribution of the blade are shown in Figure 7. These blade design parameters and unconventional airfoils were designed by NASA to optimize the rotor performance in the Martian atmosphere. To compare the performance of tandem airfoil rotors with the baseline rotor, the solidity between rotors is kept constant. Therefore, the tandem airfoil rotors are two-bladed rotors and the chord distribution of the upstream and downstream blade are the same as the baseline rotor blade.

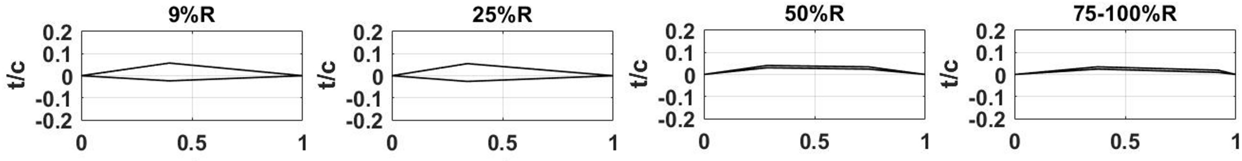

Figure 6: Unconventional Airfoils designed by NASA [17].

To conduct a performance analysis of the Mars rotor, an in-house lifting-line/Blade Element Momentum Theory (BEMT) model was used with 2D airfoil decks in this stage of the study to carry out rapid performance analysis of a large number of rotor designs. In this rotor model, the tandem airfoils in a blade are modeled as a single airfoil. The upstream and downstream airfoil combined lift, drag, and pitch moment coefficients are put into a C81 airfoil deck file. The interaction between the airfoils is considered in the CFD model, however, the difference in angle of attack due to the difference in induced velocity is not accounted for in the current model. This assumption will be removed later on in a detailed study of chosen cases by using a free-wake-based rotor model. A comparison of the calculated Figure of Merit of the baseline rotor between the present model and the data in Ref [9] is shown in Figure 8. The agreement is acceptable considering the difference in the inflow model.

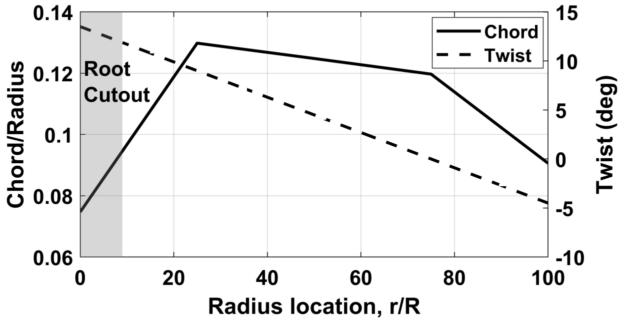

Figure 7: Chord and Twist Distribution designed by NASA [2].

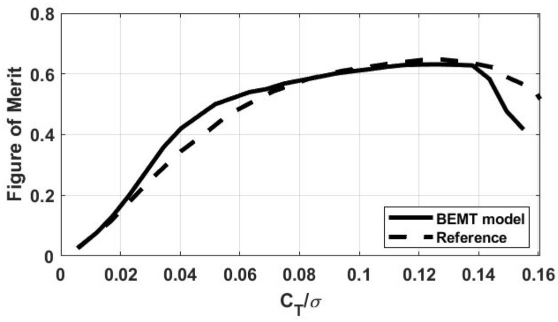

Figure 8: Variation of Figure of Merit with blade loading.

2.3 Performance Prediction Methodology

The aerodynamic performance of tandem rotor configurations was evaluated using a custom MATLAB-based Blade Element Momentum Theory (BEMT) model. The framework integrates spanwise-resolved blade element analysis with induced velocity predictions to estimate thrust, power consumption, and figure of merit (FM). Aerodynamic input data are provided in C81-format tables derived from 2D CFD simulations, encompassing both conventional and tandem airfoil polars.

Each tandem configuration is represented as a single equivalent airfoil, with aerodynamic coefficients (C_l, C_d, C_m) extracted from the CFD-derived combined performance of upstream and downstream elements. While interaction effects are inherently captured in the CFD inputs, the model assumes uniform induced velocity and angle of attack across each blade section, consistent with a lifting-line implementation. This assumption facilitates efficient parametric sweeps but does not account for intra-tandem differential loading or wake distortion.

Model Assumptions

- Blades are modeled as rigid, with no structural deformation or aeroelastic effects.
- Induced velocity is solved iteratively via a hover trim loop, assuming axisymmetric inflow and neglecting non-uniformities from wake curvature or control input.
- Martian atmospheric properties (density, viscosity, speed of sound) are held constant.
- Tandem airfoils are treated as equivalent single sections based on combined CFD-derived polars; internal element-wise flow differences are not resolved.
- Tip loss is incorporated using conventional correction methods; unsteady and dynamic stall phenomena are not modeled.

Validation and Scope

The model was benchmarked against published performance data for Mars rotor concepts, including NASA's reference blade designs. Agreement was verified across (C_T/σ), (C_P/σ), and FM metrics, for both single and tandem airfoil cases. Particular attention was given to confirming sensitivity to geometric parameters such as twist, taper, and tandem spacing. While limited in its ability to resolve wake-airfoil interaction and unsteady effects, the model proved effective in mapping performance trends and supporting configuration selection within a preliminary design context.

Do we have all there data? If you claim it, you have to show it. Please remove the contents that do not have supports.

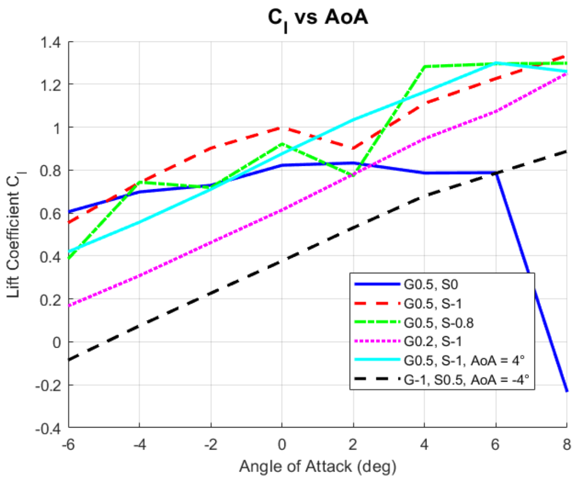

Figure 9: Coefficients of Lift for Tested Airfoils

2.4 Current Model

lifting-line/free wake aerodynamics. lifting-line model with 2-D unsteady flow airfoil C81 tables and free wake. The free wake is a time-marching version of Maryland Free Wake [**?**]. For the present study, a single rolled-up vortex is used, released from the blade tip quarter-chord. The vortex strength equals 55% maximum circulation outboard of 50% span, and the vortex core is 10% of the tip chord when formed with a growth factor of 0.05. These numbers are set empirically based on experience validation with single and coaxial rotors of a similar scale. In hover, 12 turns of wake with 15° azimuth angle discretization are used. A full span Weissinger-L near wake model [**?**] is used 30° behind each blade after which the wake rolls up.

The modifications include to model the TAC Mars rotor: 1. separate the cross sections in the TAC blade into upstream and downstream airfoils. Airfoil data tables of upstream and downstream airfoils are extracted from TAC CFD analysis. Since the upstream and downstream airfoils are modeled and analyzed as a whole in CFD, the interaction among them is included in the airfoil table. 2. Compare to the initial rotor aerodynamic model, the current model using free-wake to calculate the induced velocity of the rotor. There are two rolled-up vortices released from the blade tip, one from the upstream tip, and the other from

3 Aerodynamics of Tandem Airfoils (Ricson, Thomas)

3.1 Airfoils Polars (Thomas)

Cl, Cd, Cm trends

Just figue, no description in this section 3.1? Include the Ma number, Re number, AoA range, etc.

Plot the upstream and downstream Cl, Cd, Cm separely. These can relate to the flow field and have a discussion.

3.2 Flow field characteristic (Ricson)

The Martian atmosphere leads to flow behaviors that diverge significantly from those observed in Earth based rotorcraft operations. The low Reynolds numbers encountered by Martian rotors promote laminar to transitional boundary layer development, reduce convective transport, and weaken vortex dissipation. These effects not only alter lift generation, but also increase sensitivity to separation and stall, particularly at high angles of attack. To investigate how tandem aerofoil configurations might mitigate these challenges through aerodynamic interaction, pathline visualizations of pressure coefficient and velocity magnitude were generated to represent the low reynolds martian case.

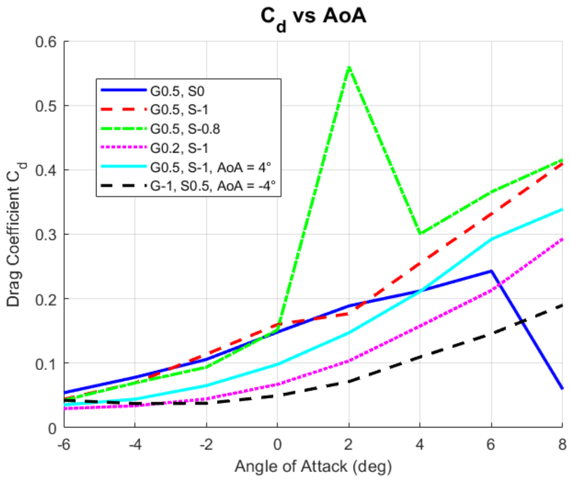

Figure 10: Coefficients of Drag for Tested Airfoils

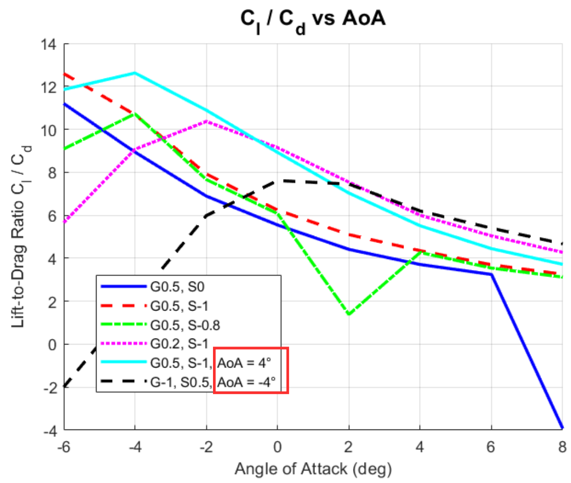

Figure 11: Lift/Drag for Tested AIrfoils

The 4 and -4 deg in these plots are not AoA (in the legend). It is the decalage angle.

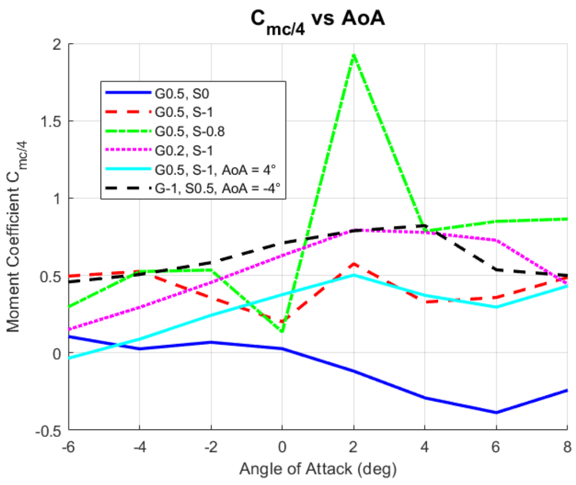

Figure 12: Coefficients of Moment for Tested Airfoils

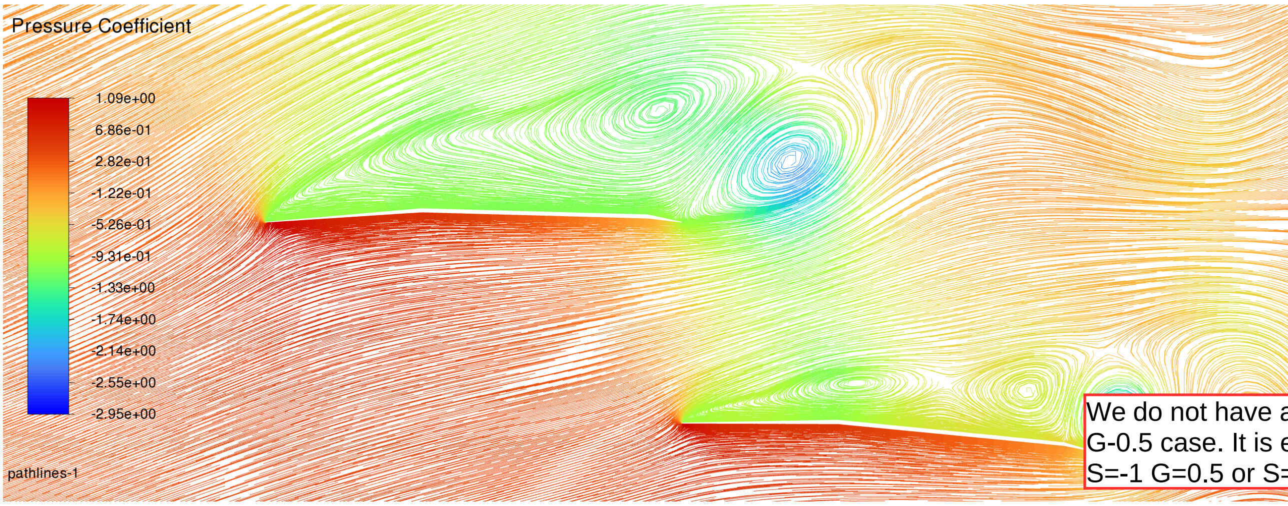

We do not have a S-1 G-0.5 case. It is either S=-1 G=0.5 or S=1 G=-0.5

Figure ?? presents pathlines colored by pressure coefficient (Cp) for a tandem aerofoil arrangement (S=-1, G=-0.5, D=4) operating at a high angle of attack (16°) under low Reynolds number conditions, representative of Martian flight. The upstream aerofoil exhibits a coherent suction peak on the upper surface, indicating largely attached flow across its chord. The resulting downwash impinges on the leading edge of the trailing aerofoil, inducing a significant pressure recovery and re-energization of the boundary layer. This is especially evident in the reduced pressure gradient near the nose of the aft aerofoil, where Cp values shift from strongly negative to near-neutral characteristic of a slot-effect acceleration zone. The narrow spacing between elements drives flow compression in the inter-foil region, contributing to local velocity amplification and delaying separation on the rear aerofoil's suction side. Although recirculating regions with low Cp are observed downstream of the rear element indicating partial separation the system as a whole retains coherent streamlines and favorable pressure gradients, enabling continued lift production despite the high incidence and low Reynolds number environment.

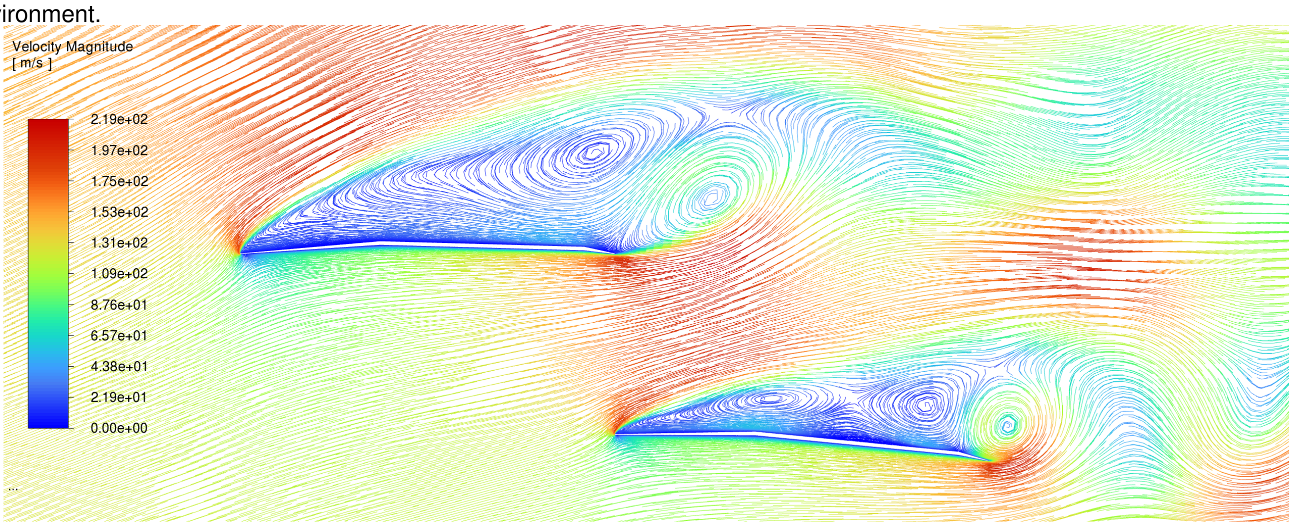

Complementing the pressure based visualization, Figure ?? displays velocity pathlines colored by magnitude. Flow acceleration between the two aerofoils is clearly visible, with velocity magnitudes exceeding 200m/s in the region between the two aerofoils . This high speed jet like flow reinforces the boundary layer on the rear aerofoil, mimicking the aerodynamic benefits of a slotted flap. Notably, the suction surface of the front aerofoil shows strong flow attachment with peak surface velocities aligned closely with the path-line curvature. While the trailing aerofoil benefits from both the induced downwash and entrained momentum. The post trailing edge region of the downstream aerofoil features well defined vortical structures and low velocity recirculation zones, consistent with partial flow separation. However, these regions do not dominate the wake, which remains largely structured and directional. The tandem configuration thus leverages inter-foil aerodynamic coupling to maintain lift and delay stall in conditions where isolated airfoils would typically experience early breakdown and reduced effectiveness.

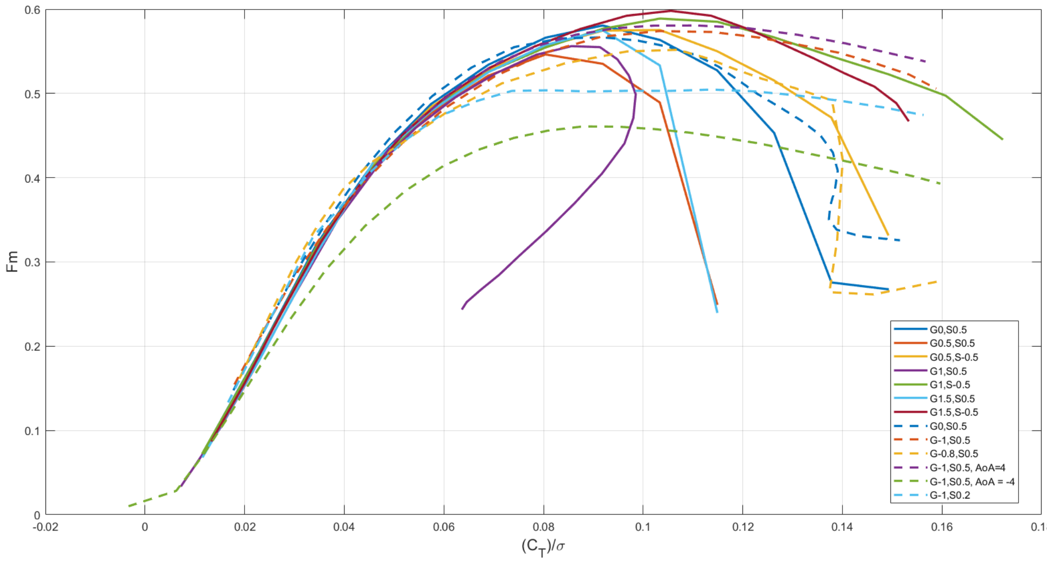

Separate this figure into multiple sets. One with only Stagger variation, one with Gap variation, and one with Decalage variation.

Provide me with th editable MATLAB file, I will need to uniform the style of the figures across the paper.

Figure 13: Figure of Merit vs Blade Loading

Legends in figure 13,14, 15 are wrong. S should be G, and G should be S. Same problem in the corresponding discussion.

4 Rotor Aerodynamic (Thomas, Lex)

4.1 Rotor performance (Thomas)

4.1.1 Figure of Merit vs Blade Loading

Figure X compares the aerodynamic performance of multiple tandem airfoil configurations under varying geometric parameters, with a focus on the Figure of Merit (FM) as a function of blade loading (C_T/σ). This analysis reflects the influence of gap (G), stagger (S), and angle of attack (AoA) on rotor efficiency.

Configurations featuring symmetric positive stagger, such as G = 0.5, S = 0.5 and G = 1.5, S = 0.5, consistently demonstrate high peak FM values and sustained performance across a wide loading range. These results affirm the beneficial aerodynamic interaction between upstream and downstream elements in well-aligned tandem setups. Specifically, positive stagger allows for favorable pressure field interaction and improved flow reattachment on the aft airfoil, mitigating early boundary layer separation.

In contrast, negatively staggered configurations—e.g., G = 0.5, S = -0.5 and G = 1.5, S = -0.5—suffer from premature degradation in FM, particularly beyond moderate loading levels. This trend confirms that rearward placement of the aft airfoil introduces detrimental wake interference, disrupting the pressure recovery process and triggering early stall. These behaviors are consistent with unsteady flow separation mechanisms exacerbated by unfavorable aft-aligned spacing.

The influence of angle of attack is illustrated through the G = 1, S = 0.5 cases at AoA = $+4^\circ$ and -4°. The $+4^\circ$ case offers a slight improvement in peak FM, maintaining similar performance trends to its unmodified counterpart, suggesting mild enhancement in lift due to better alignment with incoming flow. However, the -4° case shows a notable drop in FM and earlier stall onset, indicative of increased adverse pressure gradients and weakened flow attachment, particularly on the aft airfoil. These results validate the high sensitivity of tandem systems to inflow incidence and airfoil orientation.

Other configurations like G = 0, S = 0.5 and G = 0.8, S = 0.5 present moderate peak FM values but display a sharp decline post-peak, indicative of early stall. These results suggest that while reduced gap can strengthen near-field aerodynamic coupling at lower loads, it can also intensify wake interference at higher blade loading, diminishing downstream airfoil effectiveness.

Notably, the G = 1, S = -0.5 configuration emerges as a top-performing setup, maintaining high FM across an extended range of (C_T/σ). This aligns with findings from your dissertation, which identified this configuration as optimal due to its delayed stall onset and effective aerodynamic load distribution along the span. Its consistent performance indicates an effective balance between pressure recovery, induced velocity profiles, and minimized interference between elements.

Overall, these trends reinforce that aerodynamic efficiency in tandem rotor systems is critically dependent on both geometric configuration and flow alignment. Positive stagger and sufficient gap promote beneficial interactions, while negative stagger or improper incidence can induce severe performance penalties. Design strategies must therefore prioritize configurations that maintain coherent wake structures, support reattachment on the downstream element, and align airfoil

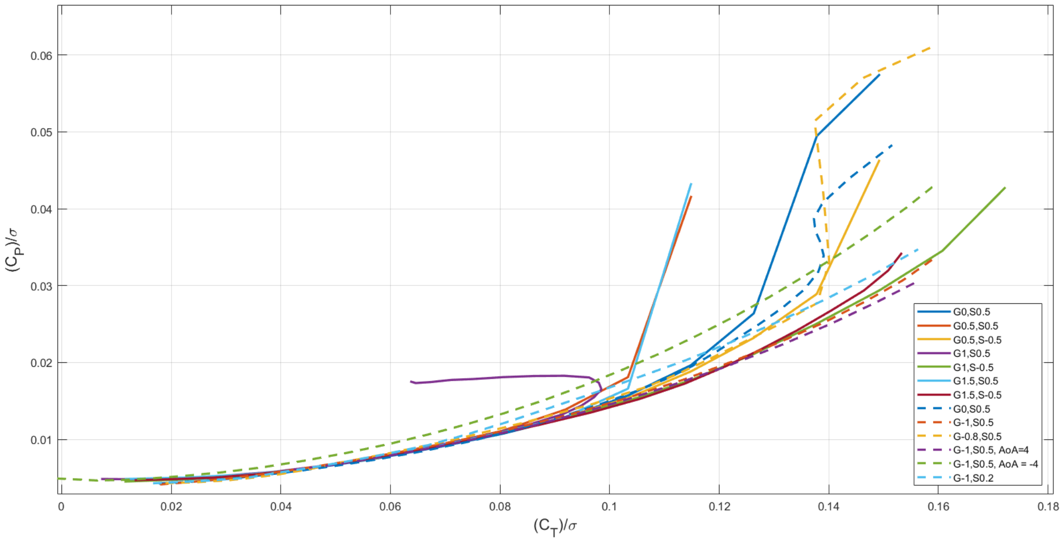

Figure 14: Power Coefficient vs Blade Loading

orientations with local inflow to maximize thrust efficiency and stall resistance under Martian conditions.

4.1.2 Power Coefficient Offset vs Blade Loading

Figure X. Variation of Power Coefficient per Unit Solidity (C_P/σ) vs. Blade Loading (C_T/σ) for Tandem Airfoil Configurations

Figure X presents the variation of power coefficient per unit solidity, (C_P/σ), as a function of blade loading, (C_T/σ), for a range of tandem airfoil configurations. As expected, all cases exhibit a generally increasing trend, reflecting the rising power requirements associated with higher thrust output. However, the rate and nature of this increase differ significantly between configurations, revealing key insights into their aerodynamic efficiency and flow behavior under elevated loading.

Configurations with symmetric geometry and moderate gap/stagger values—notably G = 0.5, S = 0.5 and G = 1.5, S = 0.5—demonstrate the most favorable performance, showing a more gradual slope in the (C_P/σ) vs. (C_T/σ) relationship. These curves remain smooth and continuous, indicating effective lift generation with minimal induced or profile power penalties. This suggests that well-aligned tandem setups preserve flow attachment and delay the onset of separation, enabling higher thrust-to-power efficiency over an extended operating range.

In contrast, negatively staggered configurations, such as G = 0.5, S = -0.5 and G = 1.5, S = -0.5, exhibit a steeper rise in power coefficient beyond moderate blade loading. This behavior reflects increased aerodynamic losses, likely due to early onset of separation on the aft airfoil, poor wake interaction, and heightened drag. The sharp curvature and inflection points in these curves serve as markers of reduced flow coherence and growing inefficiencies at higher collective pitch settings.

The influence of angle of attack (AoA) is also evident. The configuration with G = 1, S = 0.5 at AoA = -4° shows an early and rapid increase in power consumption, even at relatively low (C_T/σ) values. This indicates poor aerodynamic alignment, where adverse pressure gradients and misaligned incidence induce early flow breakdown and high drag. Conversely, the same geometry at AoA = $+4^\circ$ maintains lower (C_P/σ) values across a broader loading range, suggesting improved aerodynamic alignment and flow recovery. However, the performance gains from AoA adjustment remain limited compared to the impact of favorable geometry.

Overall, this analysis highlights the importance of aerodynamic harmony between geometry and inflow. Configurations with positive stagger and sufficient gap consistently deliver lower energy expenditure for a given thrust, as evidenced by their flatter and more efficient power-loading curves. Conversely, poorly aligned or negatively staggered setups incur nonlinear penalties, requiring significantly more power for marginal thrust gains. These results underscore that tandem rotor performance is not solely dictated by peak thrust but also by how efficiently that thrust is generated—making (C_P/σ) a critical complementary metric to the figure of merit in rotor optimization.

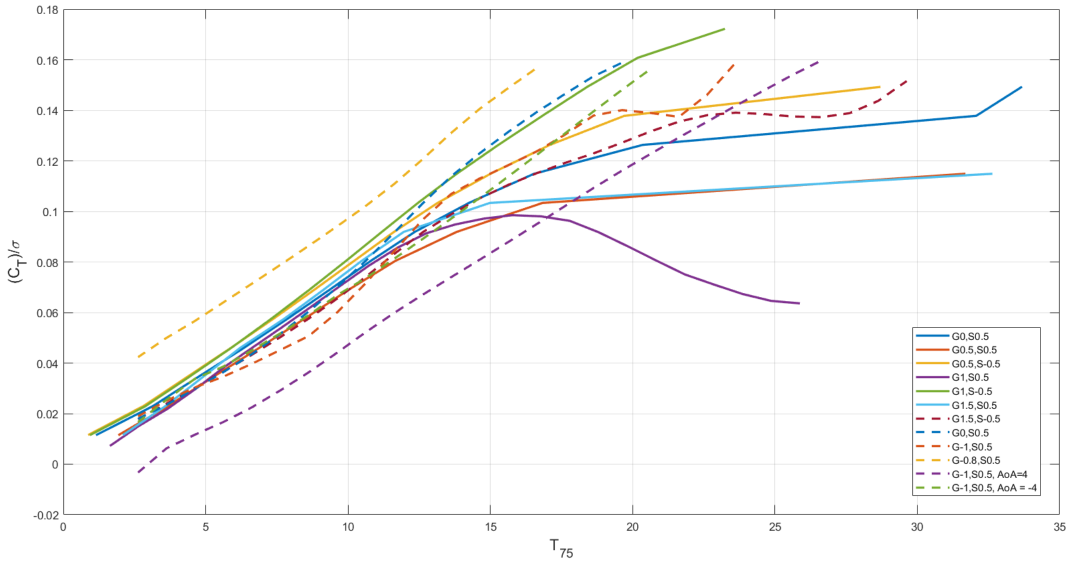

Figure 15: Blade Loading vs Collective Pitch

\theta_75 is called collective pitch

Chang T25 to \theta_25

4.1.3 Blade Loading vs collective blade pitch angle measured at 75% of the rotor blade radius.

Figure X illustrates the relationship between blade loading (C_T/σ) and the effective pitch angle at 75% blade span, T_{75}, across a variety of tandem airfoil configurations. This plot provides insight into the thrust-generating efficiency of each design as collective pitch is increased. A steeper and more sustained growth in (C_T/σ) with respect to T_{75} generally indicates more effective lift generation and better aerodynamic coupling within the tandem system.

Configurations such as G = 1.5, S = 0.5 and G = 1, S = -0.5 demonstrate strong thrust production across the pitch range, with loading continuing to increase smoothly beyond $T_{75} = 20^\circ$. This indicates robust aerodynamic performance and delayed stall onset, supporting the conclusion that sufficient gap and favorable stagger contribute to improved flow behavior, particularly in the aft airfoil.

By contrast, configurations with negative stagger (e.g., G = 0.5, S = -0.5) show early saturation or decline in (C_T/σ), particularly beyond $T_{75} \approx 15^\circ$, a clear indication of stall or wake interference effects limiting further thrust development. The configuration G = 1, S = 0.5 shows a pronounced performance collapse beyond $T_{75} = 15^\circ \ast\ast$, likely due to boundary layer separation on the downstream element, exacerbated by insufficient gap or adverse upstream flow conditions. **??

Variations in angle of attack further expose the sensitivity of tandem setups to inflow orientation. The configuration G = 1, S = 0.5 at AoA = -4° displays weakened thrust production, rising more slowly and plateauing early—evidence of flow detachment and aerodynamic inefficiency. In contrast, the same geometry at AoA = $+4^\circ$ achieves higher (C_T/σ) across the range, though it still trails behind the most efficient geometries like G = 1.5, S = 0.5.

Overall, this figure reinforces previous observations: well-spaced, positively staggered configurations are more capable of maintaining effective lift development as pitch increases. Efficient thrust performance correlates strongly with both geometric alignment and favorable aerodynamic incidence, while adverse combinations (e.g., negative stagger or misaligned AoA) accelerate the onset of nonlinearity and stall. Design optimization for tandem Mars rotors should therefore prioritize spacing and orientation that promote stable, linear thrust generation well into higher pitch ranges.

4.2 Influence of TAC on Rotor (Lex)

induced velocity

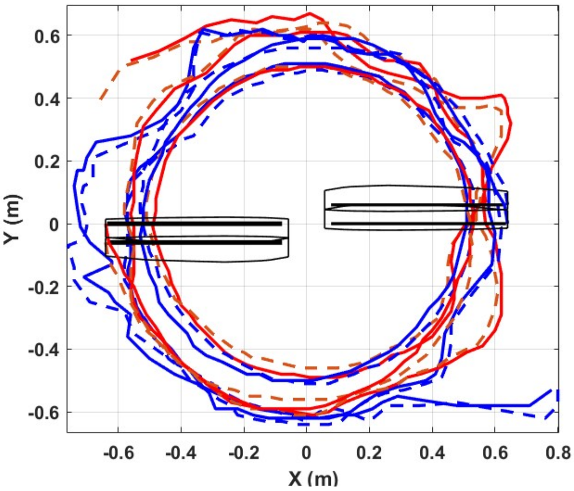

Figure 16: TAC rotor tip wake (top view).

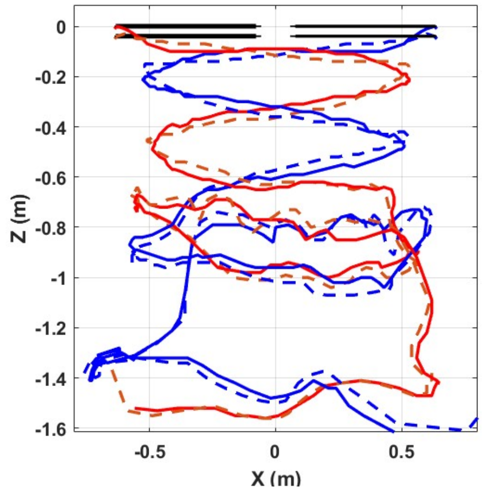

Figure 17: TAC rotor tip wake (side view).

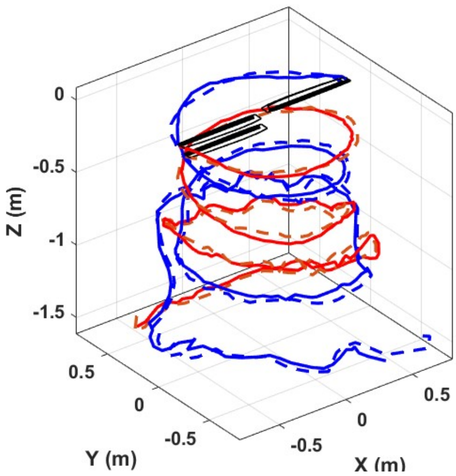

Figure 18: TAC rotor tip wake (Isometric view).

5 RESULTS AT TIME OF SUBMISSION (Will be replaced by new sections)

5.1 Tandem Airfoils

At the current stage, the study focuses on the tandem airfoils consisting of two identical double-sharp-edge airfoils at $75\%R$, and the decalage kept at zero. The gap is positive when the upstream airfoil is beneath the downstream airfoil. Figures 19 and 20 show the comparison of lift varies with the configuration parameters. All of the configurations with an upstream airfoil beneath the downstream airfoil generate less lift than the single airfoil. However, the tandem airfoil configuration with one chord length of stagger and upstream airfoil above the downstream airfoil shows a higher maximum lift coefficient than the single airfoil. In this case, the upstream airfoil contributes more than the downstream airfoil. On the other hand, all of the tandem airfoils studied show a lower lift-to-drag ratio (Figure 21). The total pitch moment is shown in figure 22. It is indicated that the configuration with a higher maximum lift results in a higher nose-up moment.

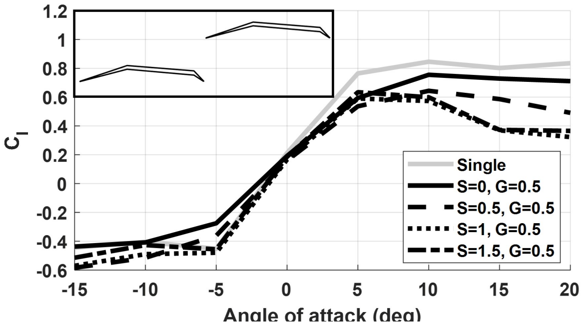

Figure 19: Lift coefficient (upstream airfoil beneath downstream).

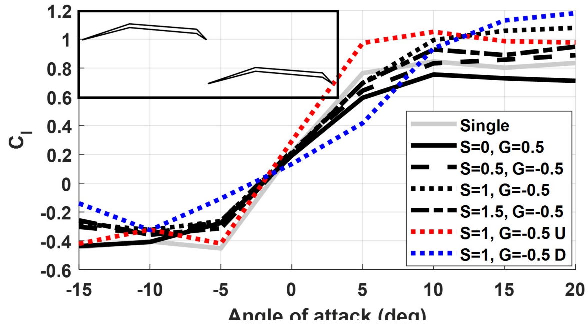

Figure 20: Lift coefficient (upstream airfoil above downstream).

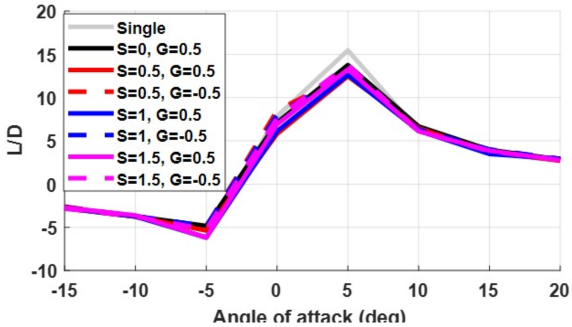

Figure 21: Lift-to-drag ratio.

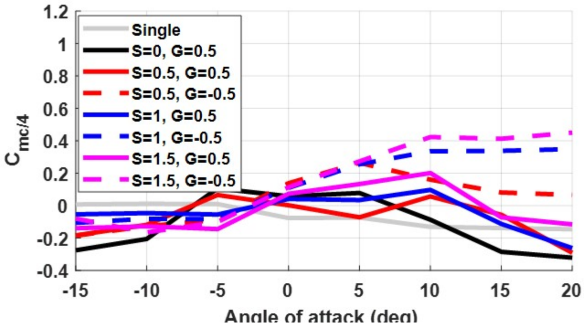

Figure 22: Moment coefficient.

5.2 Rotor performance

To isolate the impact of difference tandem airfoils, an uniform airfoil (double-sharp-edge airfoil at $75\%R$) baseline rotor was used, shown as the grey solid line in Figure 23 and 24. The hover performance of the rotor with multiple tandem airfoils is compared (collective pitch from 2° to 20°). The Figure of Merit decays with the upstream airfoil located beneath the downstream airfoil. Moreover, the maximum blade loading also decreased. When the upstream airfoil is placed above the downstream airfoil, the maximum Figure of Merit first increases with stagger as it grows from 0.5 chord to 1 chord then decreases when stagger grows further. And the maximum blade loading continues to increase with the collective. It is clear that the tandem airfoil configuration with 1 chord stagger and -0.5 gap, among the current cases, has the best improvement to the rotor performance.

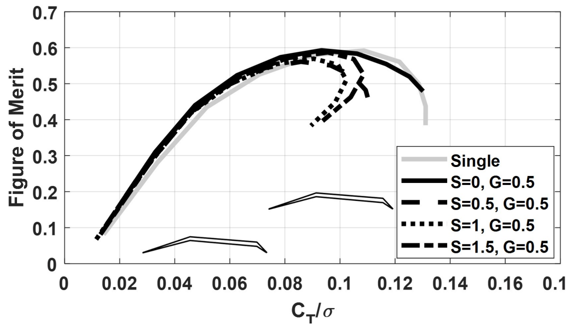

Figure 23: Figure of Merit (upstream airfoil beneath downstream).

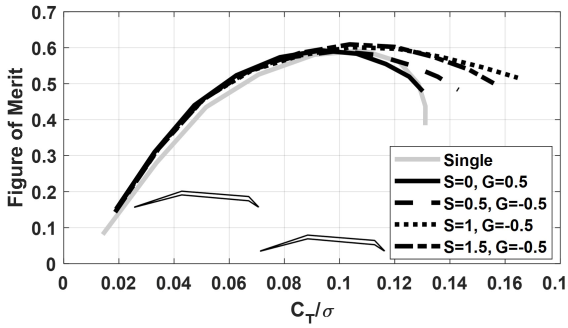

Figure 24: Figure of Merit (upstream airfoil above downstream).

6 CONCLUSIONS

7 EXPECTED DEVELOPMENTS

Of the four unconventional airfoils described in the rotor modeling section, the analysis of stagger and gap is almost completed, and the investigation of the decalage angle is underway. On the rotor side, performance analysis with all four tandem airfoils is next to be carried out, as well as the particularly important study of the aerodynamic blade root control pitch moment. The model needed to carry out forward flight analysis is also in place. Once all the tandem airfoil configurations are acquired and processed, the primary emphasis will be on the understanding of the influence of additional in-plane velocity due to the cyclic control during forward flight and any deficiencies found in the predictive tools. These, along with the data, will be documented in detail in the final paper.

Aknowledgments

Copyright Statement

References

[1] H. Cummings, B.N.P. Perez, W. Koning, W. Johnson, L. Young, F. Haddad, E. Romander, J. Balaram, T. Tzanetos, J. Bowman, and L. et al. Wagner. Overview and introduction of the rotor optimization for the advancement of mars exploration (roamx) project. San Jose, CA, 25-27 January, 2022. Transformative Vertical Flight.

[2] W. Johnson, S. Withrow, L. Young, C. Malpica, W. J. F. Koning, W. Kuang, M. Fehler, A. Tuano, A. Chan, A. Datta, C Chi, R Lumba, D Escobar, J. Bob Balaram, T Tzanetos, and H. F. Grip. Mars science helicopter conceptual design. NASA-TM—2020–220485, March 2020.

[3] J. Winslow, H. Otsuka, B. Govindarajan, and I. Chopra. Basic understanding of airfoil characteristics at low reynolds numbers $(10^4–10^5)$. *Journal of Aircraft*, 55(3):1050–1061, 2018.

[4] W. J. Koning, E.A. Romander, and W. Johnson. Low reynolds number airfoil evaluation for the mars helicopter rotor. ARC-E-DAA-TN53889, May 2018.

[5] W. J. F. Koning, E. A. Romander, and W. Johnson. Optimization of low reynolds number airfoils for martian rotor applications using an evolutionary algorithm. Orlando, FL, 6-10 January, 2020. AIAA 2020-0084, SciTech.

[6] P. Munday, K. Taira, T. Suwa, D. Numata, and K. Asai. Nonlinear lift on a triangular airfoil in low-reynolds-number compressible flow. *Journal of Aircraft*, 52(3):924–931, 2015.

[7] W. J. F. Koning, N. B. Perez Perez, H. V. Cummings, T. Nagata, Y. Kanzaki, M. Kasai, M. Miyagi, T. Nonomura, K. Asai, C. Lidia, O. Buxton, and P. Vincent. Experimental results for mars rotorcraft airfoils (roamx-0201 and clf5605) at low reynolds number andcompressible flow in a mars wind tunnel. NASA–TM–20240004230, August 2024.

[8] W. J. Koning, N. B. Perez Perez, H. V. Cummings, E. A. Romander, and W. Johnson. Elisa: A tool for optimization of rotor hover performance at low reynolds number in the mars atmosphere. In *VFS 6th Decennial Aeromechanics Specialists' Conference*, Santa Clara, CA, Jan. 2024.

[9] C. Chi, R. Lumba, Y. Su Jung, and A. Datta. Aeromechanical analysis of a next-generation mars hexacopter rotor. *Journal of Aircraft*, 59(6):1463–1477, 2022.

[10] R. Lumba, C. Chi, A. Datta, W. J. Koning, N. Perez Perez, and H. Cummings. tructural design and aeromechanical analysis of unconventional blades for future mars rotorcraft. *Journal of the American Helicopter Society*, 68(4):42003–42018, 2023.

[11] H. F. Grip, D. P. Scharf, C. Malpica, W. Johnson, G. Singh, and L. Young. Guidance and control for a mars helicopter. In *AIAA Science and Technology Forum and Exposition*, Kissinger, FL, Jan. 2018. AIAA.

[12] D. F. Scharpf and T. J. Mueller. Experimental study of a low reynolds number tandem airfoil configuration. *Journal of Aircraft*, 29(2):231–236, 1992.

[13] T. Broering and Y. Lian. The effect of wing spacing on tandem wing aerodynamics. In *Applied Aerodynamics Conference*, page 4385, Chicago, IL, June 2020. AIAA.

[14] R. Jones, D. J. Cleaver, and I. Gursul. Aerodynamics of biplane and tandem wings at low reynolds numbers. *Experiments in Fluids*, 56:1–25, 2015.

[15] L. Faure, T.M. ad Hétru and O. Montagnier. Aerodynamic features of a two-airfoil arrangement. *Experiments in Fluids*, 58(146), 2017.

[16] T.M. Faure, L. Dumas, and O. Montagnier. Numerical study of two-airfoil arrangements by a discrete vortex method. *Theor. Comput. Fluid Dyn.*, 34:79–103, 2020.

[17] W. J. Koning, M. Dominguez, and W. Johnson. Mars science helicopter rotor geometry. NASA-TM—2024-0013701, November 2024.